

Radio, X-ray and gamma-ray surface brightness profiles as powerful diagnostic tools for non-thermal SNR shells

O. Petruk^{1,2}, S. Orlando³, V. Beshley², F. Bocchino³

¹*Institute for Applied Problems in Mechanics and Mathematics, Naukova St. 3-b, 79060 Lviv, Ukraine*

²*Astronomical Observatory, National University, Kyryla and Methodia St. 8, 79008 Lviv, Ukraine*

³*INAF - Osservatorio Astronomico di Palermo “G.S. Vaiana”, Piazza del Parlamento 1, 90134 Palermo, Italy*

Accepted Received ...; in original form ...

ABSTRACT

Distributions of nonthermal surface brightness of supernova remnants (SNRs) contain important information about the properties of magnetic field and acceleration of charged particles. In the present paper, the synchrotron radio, X-ray, and inverse-Compton (IC) γ -ray maps of adiabatic SNRs in uniform interstellar medium and interstellar magnetic field are modeled and their morphology is analyzed, with particular emphasis to comparison of azimuthal and radial variations of brightness in radio, X-rays, and γ -rays. Approximate analytical formulae for the azimuthal and radial profiles of the synchrotron radio and X-ray as well as the IC γ -ray brightness are derived. They reveal the main factors which influence the pattern of the surface brightness distribution due to leptonic emission processes in shells of SNRs and can account for some non-linear effects of acceleration if necessary. These approximations provide observers and theorists with a set of simple diagnostic tools for quick analysis of the non-thermal maps of SNRs.

Key words: ISM: supernova remnants – shock waves – ISM: cosmic rays – radiation mechanisms: non-thermal – acceleration of particles

1 INTRODUCTION

Non-thermal images of SNRs are rich sources of information about the properties of interstellar magnetic field (ISMF) behavior and kinetics of charged particles in vicinity of the strong non-relativistic shocks. Despite of their importance, images of SNRs – in contrast to broad-band spectra – are not well studied.

Synchrotron X-ray brightness profiles were used as diagnostic tools for the estimate of the post-shock magnetic field in some SNRs (e.g. Berezhko & Völk 2004). Radio azimuthal profiles were used for determination of some properties of SN 1006 (Petruk et al. 2009c, hereafter Paper I) and X-ray radial profiles were used to detect the shock precursor in SN 1006 and prove particle acceleration (Morlino et al. 2010).

A detailed approach to modeling the synchrotron images of adiabatic SNRs in uniform ISMF and uniform interstellar medium (ISM) is developed by Reynolds (1998). Fulbright & Reynolds (1990); Reynolds (1998, 2004) use modeled synchrotron maps of SNRs to put constraints on properties of accelerated particles. Properties of the inverse-Compton (IC) γ -ray maps are investigated and compared to radio images in Petruk et al. (2009a, hereafter Paper II).

The influence of nonuniform ISM and/or nonuniform

ISMF on the thermal X-ray morphology of adiabatic SNRs are studied in Hnatyk & Petruk (1999), on the radio maps in Orlando et al. (2007) and on the synchrotron X-ray and IC γ -ray images in Orlando et al. (2010).

All studies of SNR maps assume classic MHD and test-particle theory of acceleration. Though they neglect effects of the back-reaction of the efficiently accelerated particles, they are able to explain general properties of the distribution of the surface brightness in radio, X-rays and γ -rays. This is because the classic theory, in contrast to the non-linear one, is able to deal with oblique shocks, that is vital for synthesis of SNR images.

At present, the theory which considers effects of accelerated particles on the shock and on acceleration itself is developed for the initially quasi-parallel shocks only. One may therefore model the only radial profiles of brightness, in the rather narrow region close to the shock (in order to be certain that obliquity does not introduce prominent modifications). Effects of non-linear acceleration on the radial profiles of brightness are considered in Ellison & Cassam-Chenaï (2005); Cassam-Chenaï et al. (2005); Lee et al. (2008); Zirakashvili & Aharonian (2010).

Future studies on SNR morphology should take into account the NLA effects. Nevertheless, the classic approach is able to reveal the general properties of SNR maps de-

arXiv:1012.4579v1 [astro-ph.HE] 21 Dec 2010

terminated by MF behavior and particle acceleration. Beside that, it is important to know the properties of the ‘classic’ images because they create the reference base for investigation of the efficiency of NLA effects in the surface brightness distribution of SNRs.

In Paper I, we introduced a method to derive an aspect angle of ISMF from the radio brightness of SNR. In Paper II, we synthesized radio and IC γ -ray maps and concluded that coincidence of the position of the γ -ray and radio limbs is not a common case in theoretical models, because different parameters are dominant in determination of the radio and γ -ray brightness variations. On the other hand, radio, X-ray and γ -ray observations (Petruk et al. 2009c; Miceli et al. 2009; Acero et al. 2010) show that radio, X-ray and γ -ray limbs coincide in SN 1006. As discussed in Paper II, such coincidence might be attributed to a combination of obliquity dependences of magnetic field and properties of emitting particles, as well as orientation versus the observer.

In the present paper, we make a step forward extending our model of non-thermal leptonic emission of Sedov SNRs in uniform medium to the X-ray band. We also derive brightness profiles for representative parameters which are suited for the comparison with adiabatic SNRs. Moreover, we derive analytical approximations of the azimuthal and radial profiles of radio, X-ray and γ -ray brightness which are extremely useful to demonstrate their dependence on the acceleration parameters, magnetic field orientation and the viewing geometry; they can also be directly and very easily fitted to SNR images to derive estimations for the best-fit quantities. While the analytical approximation cannot substitute the more accurate numerical simulations, we show that they retain enough accuracy to represent an effective diagnostic tool for the study of non-thermal SNR shells.

2 RIGOROUS TREATMENT OF SYNCHROTRON AND IC EMISSION OF SEDOV SNRS

2.1 General considerations

The present paper is continuation of the study in Paper II. The model and numerical realisation are therefore similar to those used in the Paper II; the reader is referred to this paper for more details. In short, in order to investigate the properties of the leptonic emission of Sedov SNR, we use the Sedov (1959) solutions for dynamics of fluid as well as the Reynolds (1998) description of the MF behavior downstream of the shock. The use of analytical solutions allows us to reduce the computational time considerably. We follow Reynolds (1998) also in calculation of the evolution of the distribution function $N(E)$ of relativistic electrons downstream of the shock (see Appendix A for details).

The ISMF orientation versus observer is described by the aspect angle ϕ_o , an angle between ISMF and the line of sight. Let us define also the obliquity angle Θ_o as the angle between ISMF and the normal to the shock, and the azimuth angle φ in the projection plane which is measured from the direction of the component of ISMF in the plane of the sky (see Fig. 1 in Paper II).

The compression factor for ISMF at the shock front σ_B is modulated from unity at parallel shock to $\sigma = (\gamma + 1)/(\gamma -$

1) at perpendicular one (where γ is the adiabatic index), in agreement with Reynolds (1998).

At the shock, the energy spectrum of relativistic electrons is taken to be $N(E) = KE^{-s} \exp(-(E/E_{\max})^\alpha)$, where E_{\max} is the maximum energy of electrons, s the spectral index, K the normalization, free parameter α regulates the rate of the spectrum decrease around the high-energy end¹. Evolution of the ‘electron injection ability’ of the shock is represented as $K \propto V^{-b}$ where V is the shock velocity, and b is a constant. The variation of the distribution $N(E)$ over the surface of the SNR and its evolution downstream of the shock are calculated as described by Reynolds (1998). Following Reynolds (1998), we synthesize the synchrotron and IC emission, considering each of the three cases of variation of electron injection efficiency with the shock obliquity (quasi-perpendicular, isotropic, and quasi-parallel particle injection) and each of the three alternatives for time and spatial dependence of E_{\max} (time-limited, loss-limited and escape-limited with a gyrofactor η as a parameter; it is a ratio of the mean free path of a particle to its gyroradius). Both the synchrotron and the IC losses are included as channels for the radiative losses of relativistic electrons, though the IC losses are quite small comparing to synchrotron due to large MF considered.

The surface brightness is calculated by integrating emissivities along the line of sight within the SNR. The emissivity of electrons is given by

$$q(\varepsilon) = \int_0^\infty N(E)p(E, \varepsilon)dE \quad (1)$$

where ε is the photon energy and p is the spectral distribution of synchrotron or IC radiation power of electron. We assume that information about orientation of B inside SNR is lost because of turbulence, in practice, we use an average aspect angle downstream. The distribution p is calculated with the use of the analytical approximation developed by Petruk (2009, see also Paper II).

2.2 Images

The resulting synchrotron radio images and the IC γ -ray images synthesized by our model have been already presented in Paper I and Paper II. Therefore, we present here only the X-ray images (see Fig. 1), adding appropriate references to the previous work to let the reader do a quick comparison.

The pattern of synchrotron X-ray brightness of SNR is in general similar to the radio one. In most cases, the bright X-ray limbs or other features are located in the same azimuth as in the radio images. The only differences appear

¹ A number of observations (Ellison et al. 2000, 2001; Lazendic et al. 2004; Uchiyama et al. 2003) reveal evidence of broadening of the high-energy cut-off, i.e. $\alpha < 1$. Such broadening should be attributed to the physics of acceleration (Petruk 2006), rather than to the effect of superposition of spectra in different conditions along the line of sight as it was suggested initially by Reynolds (1996). From other side, theoretical model of Zirakashvili & Aharonian (2007) demonstrates that it should be $\alpha = 2$ for the loss-limited models, whereas in practice, taking the time evolution into account it could be between 1 and 2 (Schure et al. 2010). Also Kang & Ryu (2010) suggest that $\alpha > 1$.

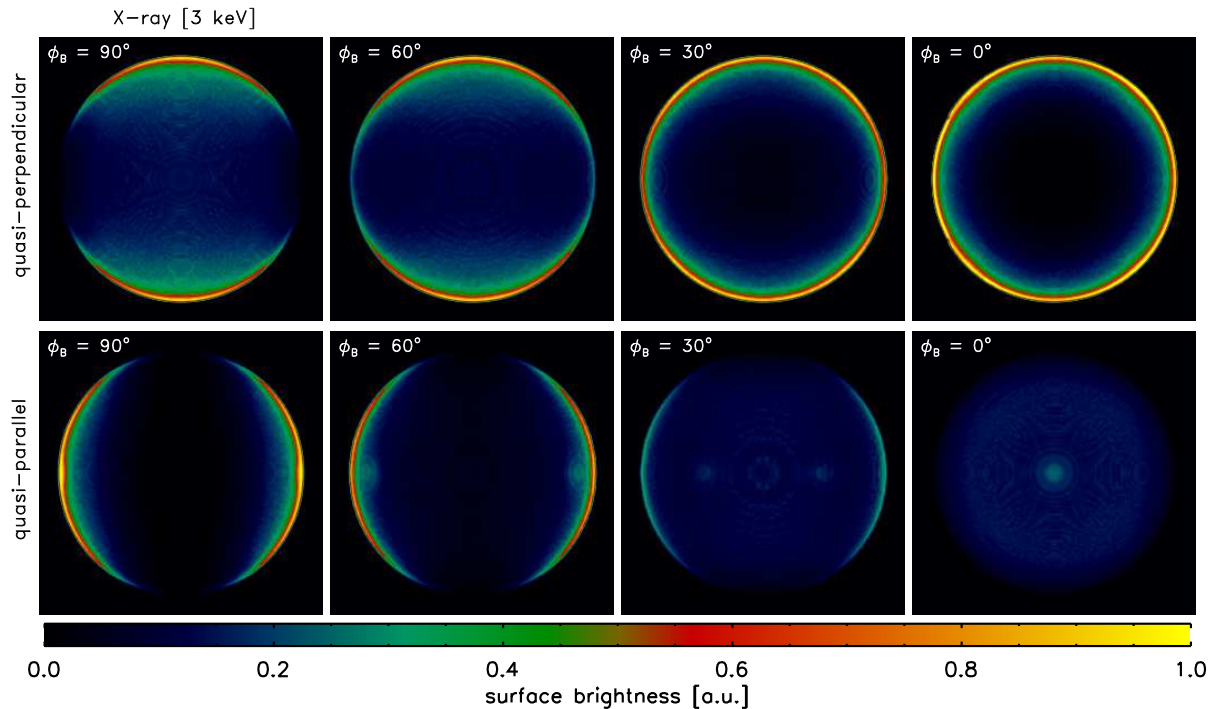


Figure 1. Maps of synchrotron X-ray surface brightness synthesized for different aspect angles (labeled in the upper left corner of each panel). The figure shows the quasi-perpendicular (top), and quasi-parallel (bottom) particle injection models. The model of E_{\max} is time-limited with $\eta = 1$. Calculations are done for $E_{\max\parallel} = 26$ TeV, $B_o = 30$ μ G, $s = 2$, $\alpha = 0.5$, $b = -3/2$. The ambient magnetic field is along the horizontal axis.

due to radiative losses which modify downstream distribution of the electrons emitting in X-rays (thus the features of brightness are radially thinner) and due to variation of E_{\max} over the SNR surface. In the radio (see Fig. 4 in Paper II) as also in the X-ray band, the remnant shows two symmetric bright lobes (for $\phi_o = 90^\circ$) in all the injection models with the maxima in surface brightness coincident in the two bands. The maxima are located at perpendicular shocks in the quasi-perpendicular and isotropic models (i.e. where B is higher), and at parallel shocks in the quasi-parallel model (i.e. where emitting electrons are only presented). The lobes are much radially thinner in X-rays than in radio because of the large radiative losses at the highest energies that make the X-ray emission dominated by radii closest to the shock.

The X-ray morphology of SNR is different for different aspect angles (Fig. 1, cf. with Figs. 4, 5 and 6 of Paper II for radio and γ -ray images, respectively). In the case of quasi-perpendicular injection, the morphology is bilateral (two lobes) for large aspect angles ($\phi_o > 60^\circ$, i.e. the component of ISMF in the plane of the sky is larger than that along the line of sight) and almost ring-like for low aspect angles ($\phi_o < 30^\circ$; see Fig. 1) with intermediate morphology between 30° and 60° . In the case of quasi-parallel injection, the remnant morphology in the radio band is known to be bilateral for large aspect angles and characterized by one or two eyes for low aspect angles (Fulbright & Reynolds 1990; Orlando et al. 2007). On the other hand, it is worth noting that the remnant morphology in X-rays is in general bilateral for aspect angles $\phi > 30^\circ$ and centrally bright for very low angles, indeed a rather limited set of possible cases (lower panels in Fig. 1). This happens because the

non-thermal X-ray emission originates from a very thin shell behind the shock making the effect of limb brightening in X-rays more important than in the radio band. In addition, we note that centrally bright X-ray (and radio) SNRs are expected to be much fainter than bilateral SNRs (see lower panels in Fig. 1) and consequently much more difficult to be observed. The above considerations may affect the statistical arguments generally invoked against the quasi-parallel injection (i.e. the fact that this model produces morphology which is not observed; e.g. Fulbright & Reynolds 1990; Orlando et al. 2007).

Images on Fig. 1 are calculated assuming a dependency of E_{\max} on the obliquity angle which corresponds to the time-limited model with $\eta = 1$ as introduced by Reynolds (1998), namely $E_{\max} \propto \mathcal{E}_{\max}(\Theta_o)B_o$, where $\mathcal{E}_{\max}(\Theta_o)$ is a function describing smooth variations of E_{\max} versus obliquity, and B_o is the pre-shock ISMF strength (in such a model no dependency on the shock velocity is present; Reynolds 1998). With this particular choice, E_{\max} is quite similar for different obliquities, namely $E_{\max\perp}/E_{\max\parallel} = 1.3$. Larger values of η always provide $E_{\max\perp}/E_{\max\parallel} > 1$ in this model, thus the character of azimuthal variation of brightness would be similar.

The efficiency of variation of E_{\max} with obliquity in modification of the azimuthal distribution of X-ray synchrotron brightness depends obviously on the photon energy: if the maximum contribution to the emission at given photon energy is from electrons with energy much less than E_{\max} then this effect is negligible. It is useful to introduce the reduced photon energy, as $\tilde{\epsilon} = \nu/\nu_c(E_{\max\parallel}, B_o)$ where

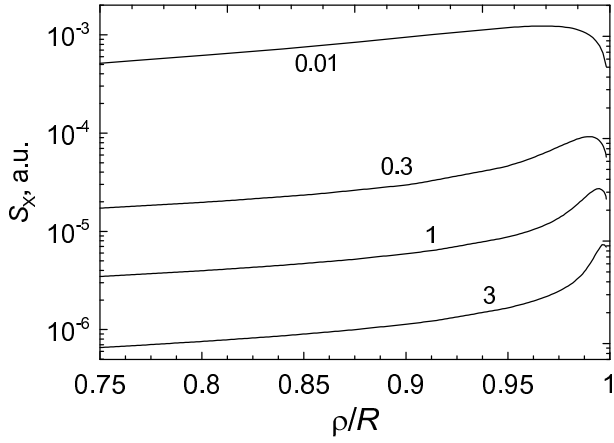


Figure 2. Radial profiles of X-ray surface brightness for different photon energies $\tilde{\epsilon}$ (marked near respective lines). Calculations are done for $\phi_o = 0$, $\varphi = 0$, $b = -3/2$, $\epsilon_{f\parallel} = 1$.

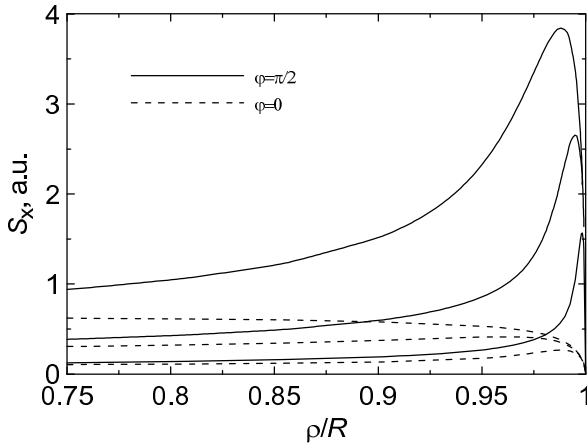


Figure 3. Effect of radiative losses (represented by $\epsilon_{f\parallel}$) on the radial profiles of X-ray surface brightness, at two azimuth. The reduced fiducial energy $\epsilon_{f\parallel} = 0.3, 1, 3$ (from below); $\phi_o = \pi/2$, $\tilde{\epsilon} = 1$, $b = 0$.

$\nu_c(E, B) = c_1 (\sin \phi) E^2 B$ is the synchrotron characteristic frequency, $c_1 = 6.26 \times 10^{18}$ cgs, or

$$\tilde{\epsilon} = 19 \epsilon_{\text{keV}} \left(\frac{E_{\text{max}\parallel}}{10 \text{ TeV}} \right)^{-2} \left(\frac{B_o}{10 \mu\text{G}} \right)^{-1}, \quad (2)$$

where ϵ_{keV} is the photon energy in keV. If $\tilde{\epsilon} = 0.29$ then most of the contribution to the synchrotron X-ray emission is from electrons with energy $E = E_{\text{max}}$.² Figs. 1 is calculated for $\tilde{\epsilon} = 2.8$, i.e. images shown are mainly due to emission of electrons with energy few times higher than $E_{\text{max}\parallel}$; the role of variation of E_{max} is therefore clearly visible in the images.

² For reference: the maximum contribution to synchrotron X-ray emission at 3 keV in MF 30 μG is from electrons with energies 72 TeV; the maximum contribution to IC γ -ray emission at 1 TeV originates from electrons with energies 17 TeV.

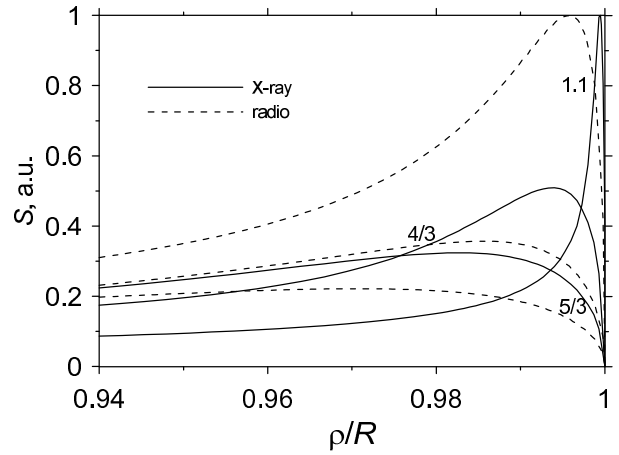


Figure 4. Radio (dashed lines) and X-ray (solid lines) radial profiles of surface brightness for the adiabatic index $\gamma = 5/3, 4/3$ and 1.1. Calculations are done for $\phi_o = 0$, $\varphi = 0$, $b = 0$, $\epsilon_{f\parallel} = 3$, $\tilde{\epsilon} = 0.3$.

2.3 Brightness profiles

In the present subsection, E_{max} is assumed to be constant in time and the same for any obliquity; in addition, isotropic injection, $s = 2$ and $\alpha = 1$ in the energy spectrum of relativistic electrons are assumed.

The radial thickness of features in the X-ray images is sensitive to the photon energy: the larger the energy the thinner the limbs (Fig. 2). This is because radiative losses \dot{E} of electrons with energy E is efficient for more energetic electrons, $\dot{E} \propto E^2$. If $\tilde{\epsilon} > 0.29$ then most of the contribution to the synchrotron X-ray emission is from electrons with energies $E > E_{\text{max}}$ where the radiative losses are of the main importance.

An important factor for emission of highly energetic electrons is the fiducial energy, which reflects the importance of radiative losses in modification of the electron distribution. It is defined as $\epsilon_f = 637 (B_s^2 t E_{\text{max}})^{-1}$ (Reynolds 1998), or

$$\epsilon_f = 13 \left(\frac{B_s}{10 \mu\text{G}} \right)^{-2} \left(\frac{E_{\text{max}}}{10 \text{ TeV}} \right)^{-1} \left(\frac{t}{1000 \text{ yrs}} \right)^{-1}. \quad (3)$$

Radiative losses are important for $\epsilon_f < 1$ and minor for $\epsilon_f > 1$. Fig. 3 demonstrates how the value of ϵ_f affects the radial profiles of X-ray brightness: the smaller ϵ_f the thinner the rim.

Our model does not include consistently the effects on shock dynamics due to back-reaction of accelerated CRs. However, we may approach the effect of shock modification by considering different values of the adiabatic index γ which is expected to drop from the value of an ideal monoatomic gas. In particular, Fig. 4 considers the cases of $\gamma = 5/3$ (for an ideal monoatomic gas), $\gamma = 4/3$ (for a gas dominated by relativistic particles), and $\gamma = 1.1$ (for large energy drain from the shock region due to the escape of high energy CRs). The shock modification results in more compressible plasma and, therefore, in the radially-thinner features of the non-thermal images of SNRs. A small distance between the forward shock and contact discontinuity (Cassam-Chenaï et al. 2008; Miceli et al. 2009) could also be attributed to $\gamma < 5/3$. Effect of the index γ on the profiles of hydrodynamical pa-

rameters downstream of the adiabatic shock is widely studied (e.g. Sedov 1959): smaller γ makes the shock compression factor higher,

$$\sigma = \begin{cases} 4 & \text{for } \gamma = 5/3, \\ 7 & \text{for } \gamma = 4/3, \\ 21 & \text{for } \gamma = 1.1, \end{cases} \quad (4)$$

and the gradient of density downstream stronger (e.g. Appendix B),

$$\bar{n}(\bar{r}) \approx \bar{r}^{\kappa_{\text{nr}}}, \quad \kappa_{\text{nr}} = \begin{cases} 12 & \text{for } \gamma = 5/3, \\ 25 & \text{for } \gamma = 4/3, \\ 88 & \text{for } \gamma = 1.1, \end{cases} \quad (5)$$

(where $\bar{n} = n/n_s$, n_s is the density immediately postshock and $\bar{r} = r/R \leq 1$). In addition to that, the X-ray (and also TeV γ -ray) brightness is modified by increased radiative losses of emitting electrons. Really, the larger compression leads to the higher post-shock MF and thus to increased losses, $\dot{E} \propto B^2$, which results in turn in the thinner radial profiles of brightness.

It is unknown how the injection efficiency (the fraction of nonthermal particles) depends on the properties of the shock. We parameterized its evolution as $K_s \propto V^{-b}$ where b is a constant. Effect of the parameter b on the radial profiles of the surface brightness is demonstrated on Fig. 5. The smaller b the thicker the profiles, because there are more emitting electrons in deeper layers, which were injected at previous times. This property affects the nonthermal emission in all bands. However, the effect is less prominent in X-rays (and in TeV γ -rays) if radiative losses are quite effective to dominate it (see Fig. 5, lines for different photon energies). This is in agreement with finding of Parizot et al. (2006) and Vink et al. (2006) who showed that, for $E > E_{\text{max}}$, the width of the synchrotron limbs does not depend on the shock velocity in the loss limited case. Instead, profiles of the radio brightness may be used to put limitations on the value of b .

In a similar fashion, the X-ray and γ -ray radial profiles are affected also by the time evolution of the maximum energy, $E_{\text{max}} \propto V^q$. However, it seems impossible to determine q from such profiles because contribution of other factors is often dominant.

An interesting feature of the synchrotron images of SNRs is apparent from Fig. 6. The maxima of the radial profiles of brightness for different azimuth are located almost at the same distance ρ from the center of projection, for radio and X-rays. Thus, the best way to analyze the azimuthal profiles of the surface brightness is to find the position ρ of the maximum for one azimuth and then to trace the azimuthal profile of brightness $S_\rho(\varphi)$ for fixed ρ .

3 EXPLICIT APPROXIMATE ANALYTICAL FORMULAE FOR SURFACE BRIGHTNESS PROFILES OF NON-THERMAL SNR SHELLS

The rigorous model discussed in the previous section is able to predict the non-thermal emission of Sedov SNR under a variety of conditions. However, in practical applications, it may be rather time-consuming to perform an extensive parameter space exploration, and the crucial dependence on

the relevant parameters of the acceleration processes may be hidden.

In order to understand how the properties of MF, electron injection and acceleration influence the brightness distribution, we derived analytic approximate formulae for the azimuthal and radial profiles of the surface brightness of adiabatic SNR. In this way, we can easily see what are the main factors which determine the pattern of the nonthermal images of SNRs, and which of them are mostly responsible for the azimuthal variation of the surface brightness and which for the radial one. This turns to be extremely useful in guiding the comparison with real observations. The analytical formulae are valid close to the shock only, but are adequate to describe azimuthal and radial variations of brightness around maxima which are located close to the edge of SNR shells.

3.1 Radio profiles

Let the evolution and obliquity variation of the electron injection efficiency be denoted as $V(t)^{-b}\zeta(\Theta_o)$ and of the obliquity variation of MF compression/amplification as $\sigma_B(\Theta_o)$; for the sake of generality we assume $\zeta(\Theta_o)$ and $\sigma_B(\Theta_o)$ to be some arbitrary smooth functions. Properties of the azimuthal and radial profiles of the radio brightness is determined mostly by (Appendix E)

$$S_r(\varphi, \bar{\rho}) \propto \zeta(\Theta_{o,\text{eff}}(\varphi, \phi_o)) \sigma_B(\Theta_{o,\text{eff}}(\varphi, \phi_o))^{(s+1)/2} I_r(\bar{\rho}) \quad (6)$$

where

$$I_r = \frac{1}{\sqrt{1-\bar{\rho}^2}} \frac{1-\bar{\rho}^{\sigma(\kappa_r+1)}}{\sigma(\kappa_r+1)}, \quad (7)$$

$\bar{\rho} = \rho/R$, σ is the shock compression ratio,

$$\kappa_r = 3b/2 + (2+s)\kappa_{\text{ad}} + 1/\sigma + s, \quad (8)$$

κ_{ad} is close to unity for $\gamma = 1.1 \div 5/3$ (Appendix B). The effective obliquity angle $\Theta_{o,\text{eff}}$ is related to azimuth φ and aspect ϕ_o as

$$\cos \Theta_{o,\text{eff}}(\varphi, \phi_o) = \cos \varphi \sin \phi_o, \quad (9)$$

the azimuth angle is measured from the direction of ISMF in the plane of the sky. Eq. (6) is a generalisation of the approximate formula derived in Paper I.

Eq. (6) shows that the azimuthal variation of the radio surface brightness $S_\rho(\varphi)$ at a fixed radius ρ of projection, is mostly determined by the variations of the magnetic field compression (and amplification, if any) σ_B and by the variation of the electron injection efficiency ζ . The radial profile $S_\rho(\rho) \propto I_r(\rho)$ is determined mostly by σ , b and s . Adiabatic index γ affects the radial and azimuthal profiles mostly through the compression factor $\sigma = (\gamma+1)/(\gamma-1)$ because κ_{ad} weakly depends on γ .

3.2 Synchrotron X-ray profiles

Let us assume that the maximum energy is expressed as $E_{\text{max}}(\Theta_o, t) \propto V(t)^q \mathcal{E}_{\text{max}}(\Theta_o)$, where q is a constant and $\mathcal{E}_{\text{max}}(\Theta_o)$, for the sake of generality, is some arbitrary function describing the smooth variation of E_{max} versus obliquity. The synchrotron X-ray brightness close to the forward shock is approximately (Appendix C)

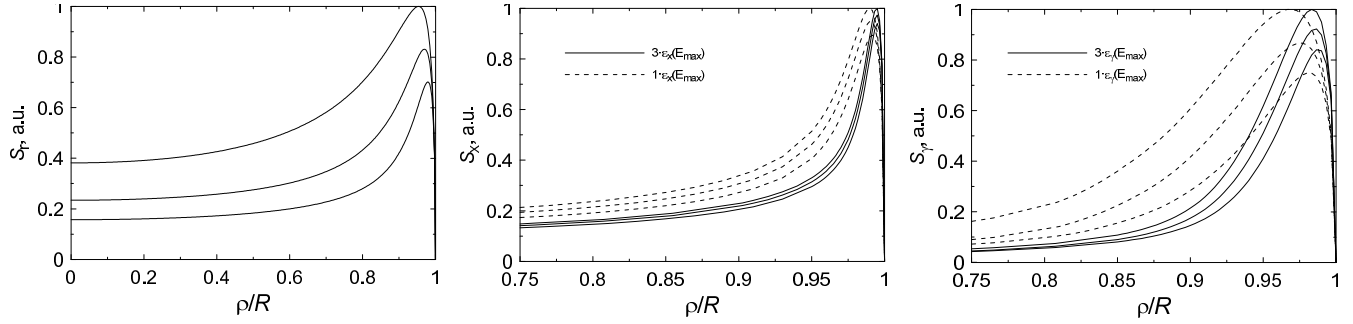


Figure 5. Evolution of injection efficiency (represented by b) and radial profiles of surface brightness in radio (left), X-rays (middle) and γ -rays (right). The parameter in relation $K_{\text{s}} \propto V^{-b}$ is $b = -3/2, 0, 2$ (from above). Other parameters are $\phi_{\text{o}} = \pi/2$, $\varphi = 0$ (for radio and X-rays) and $\varphi = \pi/2$ (for γ -rays), $\epsilon_{\text{f}\parallel} = 1$. X-ray and γ -ray profiles are shown for two photon energies: where the most contribution is from electrons with $E = E_{\text{max}}$ (dashed lines) and three times larger (solid lines); in case of X-rays, solid lines correspond to $\tilde{\epsilon} = 1$.

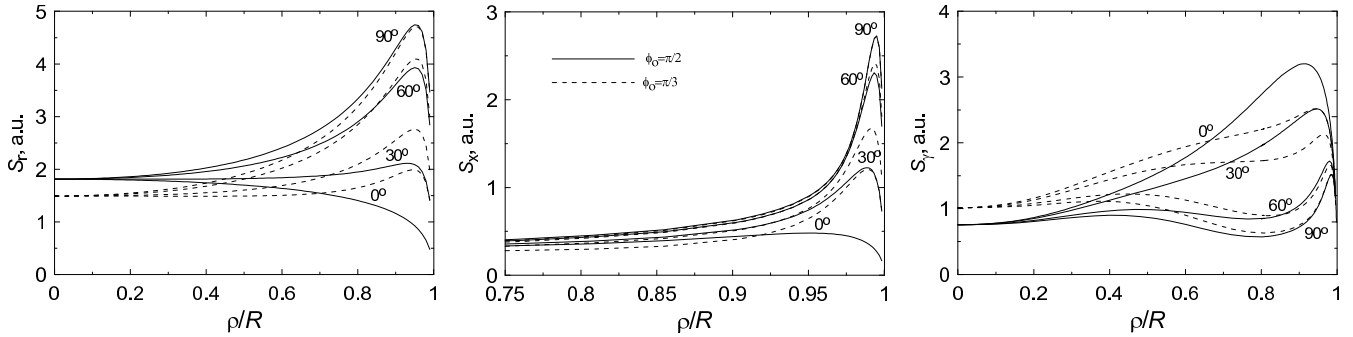


Figure 6. Radial profiles of the radio (left), X-ray (middle) and γ -ray (right) surface brightness of SNR for different azimuths: $0, \pi/6, \pi/3, \pi/2$ (marked near lines). The aspect angles are $\pi/2$ (solid lines) and $\pi/3$ (dashed lines); $b = -3/2$, $\epsilon_{\text{f}\parallel} = 1$, $\tilde{\epsilon} = 1$, γ -ray profiles are for photons with energy $0.1\epsilon_{\text{\gamma}}(E_{\text{max}})$.

$$S_{\text{x}}(\varphi, \bar{\varrho}) \propto \varsigma(\varphi) \sigma_{\text{B}}(\varphi)^{(s+1)/2} \exp \left[- \left(\frac{\epsilon_{\text{m}}(\varphi)}{\mathcal{E}_{\text{max}}(\varphi)} \right)^\alpha \right] I_{\text{rx}}(\varphi, \bar{\varrho}) \quad (10)$$

where

$$I_{\text{rx}} = I_{\text{r}}(\bar{\varrho}) I_{\text{x}}(\varphi, \bar{\varrho}) \quad (11)$$

with

$$I_{\text{x}} = \left[1 - \frac{\epsilon_{\text{m}}^\alpha(\psi + 1)\alpha}{\mathcal{E}_{\text{max}}^\alpha} \left(1 - \frac{1 - \bar{\varrho}^{\sigma(\kappa_{\text{r}}+2)} \kappa_{\text{r}} + 1}{1 - \bar{\varrho}^{\sigma(\kappa_{\text{r}}+1)} \kappa_{\text{r}} + 2} \right) \right]. \quad (12)$$

The parameter

$$\psi = \kappa_{\text{ad}} + \frac{5\sigma_{\text{B}}^2 \epsilon_{\text{m}}}{2\epsilon_{\text{f}\parallel}} - \frac{3q}{2} \quad (13)$$

is responsible for the adiabatic (the first term) and radiative (the second term) losses of emitting electrons and the time evolution of E_{max} on the shock (the third term). The reduced electron energy which gives the maximum contribution to emission of photons with energy $\tilde{\epsilon}$ is

$$\epsilon_{\text{m}} = \left(\frac{\tilde{\epsilon}}{0.29\sigma_{\text{B}}} \right)^{1/2}, \quad (14)$$

it varies with obliquity (since MF varies; electrons with different energies contribute to the synchrotron emission at $\tilde{\epsilon}$). Parameters ψ , ϵ_{m} , \mathcal{E}_{max} depend on $\Theta_{\text{o,eff}}$ and, therefore, on the aspect angle ϕ_{o} and the azimuth angle φ .

If $\epsilon_{\text{m}} \ll 1$ then Eq. (10) for the X-ray brightness transforms to Eq. (6) for the radio brightness.

The thickness of the hard X-ray radial profile is used to estimate the post-shock strength of MF in a number of SNRs (e.g. Berezhko & Völk 2004). The absolute value of MF is present in Eq. (10) through $\tilde{\epsilon}$ and ϵ_{f} , Eqs. (2), (3) which appear in ψ and ϵ_{m} , Eqs. (13), (14). In both cases, B_{s} is in combination with E_{max} (thus, the value of the electron maximum energy may affect the estimations). The idea of the method bases on the increased role of losses in X-rays due to larger MF, i.e. on the role of the second term in ψ , Eq. (13). Really, the influence of κ_{r} (i.e. of s and b) is minor in X-rays (middle panel on Fig. 5), if radiative losses affect the electron evolution downstream of the shock (i.e. for $\tilde{\epsilon} \gtrsim 0.29$, $\epsilon_{\text{f}} \lesssim 1$). The role of the first and the third terms in ψ are also minor in most cases ($q = 0$ for the time-limited and escape-limited models and unity for the loss-limited one) because the second term $\gtrsim 10$. However, the adiabatic index makes an important effect on the thickness of the profile, mostly through σ which appears in σ_{B} and in I_{x} . Being smaller than $5/3$ (that is reasonable especially in the case of efficient acceleration, which is actually believed to be responsible for the large MF), the index may compete to some extent the role of losses, used in the method for estimation of MF (see e.g. Fig. 4) that might lead to smaller estimates of MF strength.

3.3 IC gamma-ray profiles

The IC γ -ray brightness may approximately be described as (Appendix D)

$$S_{\text{ic}}(\varphi, \bar{\varrho}) \propto \zeta(\varphi) \exp \left[- \left(\frac{\epsilon_{\text{m}}}{\mathcal{E}_{\text{max}}(\varphi)} \right)^\alpha \right] I_{\text{ic}}(\varphi, \bar{\varrho}) \quad (15)$$

where

$$I_{\text{ic}}(\varphi, \bar{\varrho}) \approx \frac{1}{\sqrt{1-\bar{\varrho}^2}} \frac{1-\bar{\varrho}^{\sigma(\kappa_{\text{ic}}+1)}}{\sigma(\kappa_{\text{ic}}+1)} \quad (16)$$

$$\times \left[1 - \frac{\epsilon_{\text{m}}^\alpha \psi \alpha}{\mathcal{E}_{\text{max}}^\alpha} \left(1 - \frac{1-\bar{\varrho}^{\sigma(\kappa_{\text{ic}}+2)}}{1-\bar{\varrho}^{\sigma(\kappa_{\text{ic}}+1)}} \frac{\kappa_{\text{ic}}+1}{\kappa_{\text{ic}}+2} \right) \right],$$

$$\kappa_{\text{ic}} = 3b/2 + (2+s)\kappa_{\text{ad}} + 1/\sigma - 1. \quad (17)$$

The expression for ψ is the same as (13) but ϵ_{m} is different:

$$\epsilon_{\text{m}} = \frac{\varepsilon^{1/2}}{2(kT)^{1/2}\gamma_{\text{max}}}, \quad (18)$$

where ε is the γ -ray photon energy, T the temperature of the seed photon field, γ_{max} the Lorentz factor of electrons with energy E_{max} , or

$$\epsilon_{\text{m}} = 1.66 \left(\frac{E_{\text{max}}}{10 \text{ TeV}} \right)^{-1} \left(\frac{\varepsilon}{1 \text{ TeV}} \right)^{1/2} \left(\frac{T}{2.75 \text{ K}} \right)^{-1/2}. \quad (19)$$

Eq. (15) is a generalisation of the approximate formula derived in Paper II.

The azimuthal variation of the IC γ -ray brightness depends mostly on the injection efficiency. The role of variation of E_{max} is prominent only if obliquity dependence of injection is not strong. Parameter α , being smaller than unity, results in smaller azimuthal contrasts of synchrotron X-ray or IC γ -ray brightness comparing to model with purely exponential cut-off in $N(E)$. The radial distribution of IC brightness is determined mostly by σ , ϵ_{m} , ϵ_{f} , b and, to the smaller extend, by s and q .

3.4 Accuracy of the formulae

The approximations presented above do not require long and complicate numerical simulations but restore all the properties of nonthermal images discussed in the previous sections as well as in Papers I and II, including dependence on the aspect angle. Therefore, they may be used as a simple diagnostic tool for non-thermal maps of SNRs.

The formulae are rather accurate in description of the brightness distribution close to the shock. They do not represent centrally-brightened SNRs. Instead, they may be used in SNR shells for those azimuth φ where $\epsilon_{\text{m}} \lesssim 1$ and $\epsilon_{\text{f}} \gtrsim 0.1$, in the range of $\bar{\varrho}$ from $(1-2\Delta\bar{\varrho}_{\text{m}})$ to 1, where $\Delta\bar{\varrho}_{\text{m}} = 1-\bar{\varrho}_{\text{m}}$, $\bar{\varrho}_{\text{m}}$ is the radius (close to the shock) where the maximum in the radial profile of brightness happens. Approximations are compared with numerical calculations in respective Appendices and their applicability is discussed in details on example of the IC emission in Appendix D1.

4 DISCUSSION

Analysis of azimuthal profiles of brightness in different bands allows one to put limitations on models of injection, MF,

E_{max} . In most cases, the best way to estimate the azimuthal variation $S_\rho(\varphi)$ of the surface brightness is the following. An approximate radial profile $S_\rho(\rho)$ of the brightness should be produced for azimuth where the largest losses occur (i.e. where $\epsilon_{\text{f}} \propto (\mathcal{E}_{\text{max}}\sigma_{\text{B}}^2)^{-1}$ is smaller; e.g. at $\varphi = 90^\circ$). This allows us to find $\bar{\varrho}_{\text{m}}$ which should be used in $S_\rho(\varphi)$ in order to estimate the azimuthal variation of brightness. $\bar{\varrho}_{\text{m}}$ keeps us at maxima in the radial brightness profiles for different azimuth (Fig. 6).

Energy of electrons evolve downstream of the shock as $E(\bar{a}) = E_i \mathcal{E}_{\text{ad}} \mathcal{E}_{\text{rad}}$, where E_i is initial energy, $\bar{a} = a/R$, a the Lagrangian coordinate. Adiabatic and radiative losses of electrons in a given fluid element a are represented by functions $\mathcal{E}_{\text{ad}}(\bar{a}) \leq 1$, $\mathcal{E}_{\text{rad}}(\bar{a}) \leq 1$ respectively (Appendix A). Close to the shock, they are approximately $\mathcal{E}_{\text{ad}} \approx \bar{a}^{\kappa_{\text{ad}}}$ (κ_{ad} depends on the adiabatic index γ only and is close to unity for $\gamma = 1.1 \div 5/3$), $\mathcal{E}_{\text{rad}} \approx \bar{a}^{5\sigma_{\text{B}}^2 \epsilon_{\text{m}} / (2\epsilon_{\text{f}})}$ (Appendix B). The latter expression clearly shows that the fiducial energy ϵ_{f} is important parameter reflecting the ‘sensitivity’ of the model to the radiative losses, as it is shown by Reynolds (1998): the larger the fiducial energy the smaller the radiative losses. In fact, $\mathcal{E}_{\text{rad}} = 1$ means no radiative losses at all. Another fact directly visible from this approximation is that radiative losses are much more important at the perpendicular shock (where $\sigma_{\text{B}} = \sigma$) than at the parallel one (where $\sigma_{\text{B}} = 1$). In addition, the radiative losses depends rather strongly on the index γ : $\sigma_{\text{B}}^2 = 16$ for $\gamma = 5/3$ but $\sigma_{\text{B}}^2 = 49$ for $\gamma = 4/3$.

Note, that in the analysis above, the difference between the parallel and perpendicular shocks are only due to the compression factor σ_{B} which may be treated as ‘‘compression-plus-amplification’’ factor. Therefore, our consideration may also be applied in case of the very turbulent and amplified pre-shock field (when information about obliquity is lost) once this factor is known.

Our approximations reflects also the general ‘rule’ for IC emission: there is less IC emission where MF is stronger. Namely, the azimuthal variation is $I_{\text{ic}}(\varphi) \propto 1 - \text{const} \times \psi(\varphi)/\mathcal{F}(\varphi)^\alpha$ with $\psi \propto \sigma_{\text{B}}(\varphi)^2$: emitting electrons disappears toward the shock with larger σ_{B} because MF strength is a reason of higher losses there. Similar dependence on σ_{B} is for X-rays, Eq. (12); it is however dominated by the increased term $S_{\text{x}}(\varphi) \propto \sigma_{\text{B}}(\varphi)^{3/2}$.

TeV γ -ray image of SN 1006 demonstrates good correlations with X-ray image smoothed to the H.E.S.S. resolution (Acero et al. 2010). We mean here both the location and sizes of the bright limbs. Let us consider the polar-caps model of SN 1006. The shock is quasi-parallel around the limbs, MF azimuthally increases (in ≈ 4 times). The injection efficiency decreases (in $> 10^{-3}$ times) out of the limbs; the number of electrons emitting in X-rays and TeV γ -rays is therefore dramatically low at perpendicular shock comparing to the parallel, that is in agreement with no TeV emission at NW and SE regions of SN 1006. However, the azimuthal sizes of the limbs in X-rays and γ -rays is expected to be different, in the polar-caps model: they should be larger in X-rays. Really, azimuthal variation of \mathcal{E}_{max} is smaller than variations of ζ and $\sigma_{\text{B}}^{3/2}$; therefore, from Eqs. (10) and (15), azimuthal variations of brightness are mostly $S_{\text{x}} \propto \zeta \sigma_{\text{B}}^{3/2}$ while $S_{\text{ic}} \propto \zeta$ (see Fig. 7 for a comparison of remnant morphologies in the radio, X-ray and γ -ray bands). We hope that

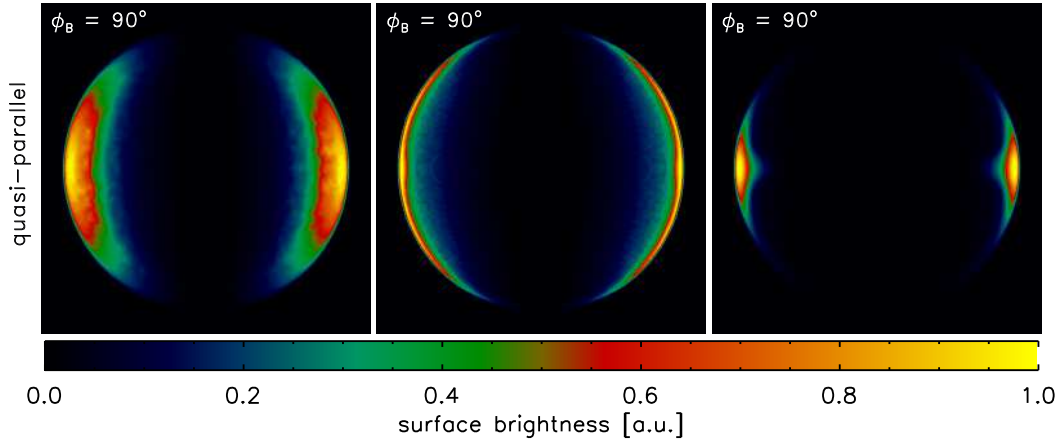


Figure 7. Radio (left), X-ray (center) and γ -ray (right) images of the polar-cap SNR, assuming quasi-parallel injection. Model parameters are the same as in Fig. 1. Different azimuthal and radial sizes of limbs in various bands are clearly visible.

future observations allow us to see if there is a difference in azimuthal sizes of the limbs in various bands.

How back-reaction of accelerated particles may modify nonthermal images of SNRs? Our formulae can restore some of these effects. In our approximations, s , in general, is allowed to vary with E , e.g. to be $s(E) = s + \delta s(E)$. The index s reflects the ‘local’ slope of the electron spectrum around ϵ_m . Therefore, if $s(E) \neq \text{const}$, the index s has to vary with azimuth because ϵ_m varies, Eq. (14). Generally speaking, such approach allows one to estimate the role of the nonlinear ‘concavity’ of the electron spectrum in modification of the nonthermal images. However, we expect that this effect is almost negligible because $\delta s(E)$ is very slow function, at least within interval of electron energies contributing to images. Another effect of efficient acceleration consists in the adiabatic index γ smaller than $5/3$. Our approximations are written for general γ . Namely, the index γ affects $S(\varphi, \bar{\nu})$ through σ . Cosmic rays may also cause the amplification of the seed ISMF. In our formulae, $\sigma_B(\Theta_o)$ represents the obliquity variation of the ratio of the downstream MF to ISMF strength, B_s/B_o . Therefore, it may account for both the compression and amplification of ISMF; for such purpose, σ_B should be expressed in a way to be unity at parallel shock.

5 COMPARISON WITH OBSERVATIONS: A WORKING EXAMPLE

The main reason for the derivation of the explicit approximations of Sect. 3 is to highlight the factors which are the most efficient in the formation of the pattern of surface brightness. However, sometimes the analytical formulae may help in estimates some of the remnant parameters. We would like to present two examples. Let us consider SN 1006, $s = 2$ (Miceli et al. 2009), $\gamma = 5/3$.

The injection efficiency is isotropic if one assumes that SN 1006 evolves in the uniform ISMF and uniform ISM (Paper I). The best-fit value of the aspect angle found from the approximate Eq. (6) is $68^\circ \pm 4.0^\circ$ (Fig. 8) while the detailed numerical calculations give $70^\circ \pm 4.2^\circ$ (Paper I).

The same approximate formula shows that the radial profile of radio brightness depends only on the value of b

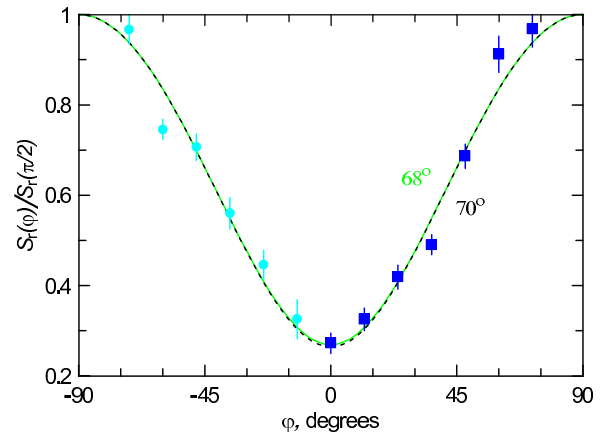


Figure 8. Azimuthal profiles of the radio brightness of SN 1006. Experimental data and the best-fit theoretical profile calculated from detailed model (dashed line) are from Paper I. Green solid line represents the best-fit profile obtained from the approximate analytical formula (6).

(which shows how the injection efficiency evolve with the shock velocity). Unfortunately, the differences between profiles for $b = -1$ and $b = 1$ are comparable with accuracy of the approximate formulae and of the experimental data; therefore, the approximation may not be used for estimations of b .

The sharpest radial profile of X-ray brightness (from Fig. 4A in Long et al. 2003) was used to estimate the strength of the post-shock MF in $\sim 100 \mu\text{G}$ (Berezhko et al. 2003). Fig. 9 shows approximate profiles for three values of MF in comparison with the Chandra profile and detailed numerical simulations (Petruk et al., in preparation). One can also see from the approximation that $B \sim 100 \mu\text{G}$ is the most appropriate value in agreement with the value found in the literature.

6 CONCLUSIONS

The present paper extends analysis of properties of the surface brightness distribution of spherical adiabatic SNRs

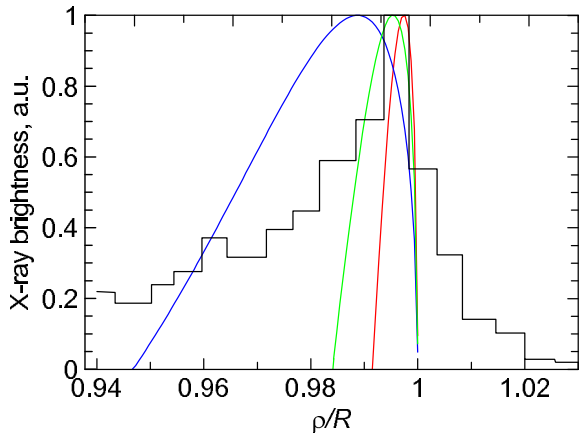


Figure 9. Radial profiles of the hard X-ray brightness of SN 1006. Experimental data (from Fig. 4A in Long et al. 2003) are shown by histogram. Profiles given by approximation (10) for $B = 50, 100, 150 \mu\text{G}$ are shown by blue, green and red lines respectively. Other parameters: $\varepsilon = 1.2 \text{ keV}$ and $\nu_{\text{break}\parallel} = 150 \text{ eV}$, $\phi_o = 68^\circ$, $\varphi = 70^\circ$, $\mathcal{E}_{\text{max}} = 2.9$, $q = 0$, $b = 0$, $\alpha = 1$.

started in Paper I (radio band) and Paper II (IC γ -rays) to the nonthermal X-rays. It also generalizes the method of approximate analytical description of the azimuthal and radial profiles of brightness introduced in these papers.

Synchrotron images of adiabatic SNR in X-rays are synthesized for different assumptions about obliquity variations of the injection efficiency, MF and maximum energy of accelerated electrons. We analyze properties of these images. Different models of electron injection (quasi-parallel, isotropic and quasi-perpendicular) as well as models of the electron maximum energy (time-limited, loss-limited and escape-limited) are considered.

The azimuthal variation of the synchrotron X-ray and IC γ -ray brightness is mostly determined by variations of ς , σ_B and E_{max} , of the radio brightness by ς and σ_B only. In general, higher B increases X-ray and decreases IC γ -ray brightness. Really, higher MF is a reason of larger losses of emitting electrons (i.e. decrease of their number) and thus of the smaller brightness due to IC process. In contrast, X-rays are more efficient there because $S_x \propto B^{3/2}$.

The radial profiles of brightness depend on a number of factors. It is quite sensitive to the adiabatic index: $\gamma < 5/3$ makes plasma more compressible. Therefore, the brightness profile is thinner due to larger compression factor, larger gradient of density and MF downstream of the shock and larger radiative losses.

The role and importance of various factors on the surface brightness in radio, synchrotron X-rays and IC γ -rays are demonstrated by the approximate analytical formulae. They accurately represent numerical simulations close to the shock and are able to account for some non-linear effects of acceleration if necessary. This makes the approximations a powerful tool for quick analysis of the surface brightness distribution due to emission of accelerated electrons around SNR shells. The application of the approximate formulae to the case of SN1006 yields measures of the aspect angle and the post-shock MF in good agreement with more accurate analysis found in the literature.

REFERENCES

- Acerro F., et al., 2010, A&A, 516, A62
 Ballet J. 2006, Adv. Space Res., 37, 1902
 Berezhko, E. G., Ksenofontov, L. T. & Völk, H. J. 2003, A&A, 412, L11
 Berezhko E. G. & Völk H. J., 2004, A&A, 419, L27
 Cassam-Chenaï G., Decourchelle A., Ballet J., Ellison D. C., 2005, A&A, 443, 955
 Cassam-Chenaï G., Hughes J. P., Reynoso E. M., Badenes C., & Moffett D., 2008, ApJ, 680, 1180
 Ellison, D. C., Berezhko, E. G., & Baring, M. G. 2000, ApJ, 540, 292
 Ellison, D. C., Slane, P., & Gaensler, B. M. 2001, ApJ, 563, 191
 Ellison D. & Cassam-Chenaï G., 2005, ApJ, 632, 920
 Hnatyk B. & Petruk O., 1999, A&A, 344, 295
 Fryxell B., Olson K., Ricker P. et al., 2000, ApJS, 131, 273
 Fulbright M. S. & Reynolds S. P., 1990, ApJ, 357, 591
 Kang, H. & Ryu, D. 2010, ApJ, 721, 886
 Lazendic, J. S., Slane, P. O., Gaensler, B. M., et al. 2004, ApJ, 602, 271
 Long K. S., Reynolds S. P., Raymond J. C., et al. 2003, ApJ, 586, 1162
 Miceli M., Bocchino F., Iakubovskiy D., Orlando S., Telezhinsky I., Kirsch M. G. F., Petruk O., Dubner G., Castelletti G., 2009, A&A, 501, 239
 Lee S.-H., Kamae T., Ellison D. C., 2008, ApJ, 686, 325
 Morlino G., Amato E., Blasi P., Caprioli D., 2010, MNRAS, 405, L21
 Orlando S., Bocchino F., Reale F., Peres G., & Petruk O., 2007, A&A, 470, 927
 Orlando S. Petruk O., Bocchino F. & Miceli M. 2010, A&A, accepted [astro-ph.HE/1011.1847]
 Parizot E., Marcowith A., Ballet J., Gallant Y. A. 2006, A&A, 453, 387
 Petruk O. 2006, A&A, 460, 375
 Petruk O., 2009, A&A, 499, 643
 Petruk, O., Beshley, V., Bocchino, F., & Orlando, S., 2009b, MNRAS, 395, 1467 (Paper II)
 Petruk O., Bocchino F., Miceli M., Dubner G., Castelletti G., Orlando S., Iakubovskiy D., Telezhinsky I., 2009b, MNRAS, 399, 157
 Petruk O., Dubner G., Castelletti G., Iakubovskiy D., Kirsch M., Miceli M., Orlando S., Telezhinsky I., 2009, MNRAS, 393, 1034 (Paper I)
 Reynolds S.P. 1996, ApJ, 459, L13
 Reynolds S. P., 1998, ApJ, 493, 375
 Reynolds S. P., 2004, Adv. Sp. Res., 33, 461
 Sedov L.I., 1959, *Similarity and Dimensional Methods in Mechanics* (New York, Academic Press)
 Schure K. M., Achterberg A., Keppens R., Vink J. 2010, MNRAS, 406, 2633
 Uchiyama, Y., Aharonian, F. A., & Takahashi, T. 2003, A&A, 400, 567
 Vink J., Bleeker J., van der Heyden K., Bykov A., Bamba A., Yamazaki R. 2006, ApJ, 648, L33
 Zirakashvili V., Aharonian F., 2007, A&A, 465, 695
 Zirakashvili V., Aharonian F., 2010, ApJ, 708, 965

APPENDIX A: EVOLUTION OF THE ELECTRON ENERGY SPECTRUM DOWNSTREAM OF THE ADIABATIC SHOCK

Relativistic electrons evolving downstream of the shock suffer from adiabatic expansion and radiative losses due to synchrotron and inverse Compton processes. Electrons are considered to be confined to the fluid element which removed them from the acceleration site (Reynolds 1998).³

Let the fluid element with Lagrangian coordinate a was shocked at time t_i . If energy of electrons was E_i at t_i , it becomes later (Reynolds 1998)

$$E = \frac{E_i}{\bar{n}(\bar{a})^{-1/3} + \mathcal{I}(\bar{a})E_i/E_f} \quad (\text{A1})$$

where the first summand in the denominator reflects adiabatic losses, the second one is due to radiative losses, $\bar{n} = n/n_s$, index 's' means 'immediately post-shock', the fiducial energy for parallel shock $E_f = 637/(B_{\text{eff},s\parallel}^2)$ cgs. The effective magnetic field is $B_{\text{eff}}^2 = B^2 + B_{\text{CMB}}^2$, $B(a)$ takes into account its evolution downstream (Reynolds 1998), $B_{\text{CMB}} = 3.27 \mu\text{G}$ strength of magnetic field with energy density equal to energy density of CMBR. B_{CMB} is introduced in order to account for the inverse-Compton losses (Reynolds 1998), therefore it is constant everywhere. The synchrotron channel dominates inverse-Compton losses if $B_s \gg B_{\text{CMB}}$.

The dimensionless function \mathcal{I} accounts for evolution of fluid during time from t_i to t ; it was initially defined as integral over time (Reynolds 1998). In case of Sedov shock, \mathcal{I} may be written in terms of spatial coordinate that is more convenient for simulations than original representation in terms of time. Namely, for uniform ISM:

$$\mathcal{I}(\bar{a}, \Theta_o, d) = \frac{5\sigma_{\text{B}}^2}{2\bar{n}(\bar{a})^{1/3}} \int_{\bar{a}}^1 x^{3/2} \bar{B}_{\text{eff}} \left(\frac{\bar{a}}{x}\right)^2 \bar{n} \left(\frac{\bar{a}}{x}\right)^{1/3} dx, \quad (\text{A2})$$

Eq. (A1) results in relations

$$E_i = \frac{E}{\mathcal{E}_{\text{ad}}\mathcal{E}_{\text{rad}}}, \quad dE_i = \frac{dE}{\mathcal{E}_{\text{ad}}\mathcal{E}_{\text{rad}}^2} \quad (\text{A3})$$

where the adiabatic and radiative losses are represented by

$$\mathcal{E}_{\text{ad}} = \bar{n}(\bar{a})^{1/3}, \quad \mathcal{E}_{\text{rad}} = 1 - \mathcal{I}(\bar{a}, \Theta_o)E/E_f. \quad (\text{A4})$$

Shocks of different strength are able to accelerate electrons to different E_{max} . Let $E_{\text{max}} \propto V^q$ where V is the shock velocity, $q = 1, 2, 0$ for loss-limited, time-limited and escape-limited models respectively (Reynolds 1998). If shock accelerates electrons to E_{max} at present time t , then, at some previous time t_i when fluid element $a \equiv R(t_i)$ was shocked, the shock was able to accelerate electrons to

$$E_{\text{max}}(t_i) = E_{\text{max}} \left(\frac{V(t_i)}{V(t)} \right)^q = E_{\text{max}} \bar{a}^{-3q/2}, \quad (\text{A5})$$

where $\bar{a} = a/R(t)$ and we used Sedov solutions. The obliquity variation of the maximum energy is given by $E_{\text{max}} = E_{\text{max},\parallel} \mathcal{E}_{\text{max}}(\Theta_o)$ with $\mathcal{E}_{\text{max}}(\Theta_o)$ independent of time.

³ Such an assumption means that we consider the advection only, not the diffusion. However, for X-ray emitting electrons, the lengthscales for advection l_{adv} and diffusion l_{dif} are comparable: $l_{\text{adv}}/l_{\text{dif}} = 0.8 - 1.1$ (Ballet 2006). Therefore, the results of the present paper are robust.

Let us assume that, at time t_i , an electron distribution has been produced at the shock

$$N(E_i, t_i) = K_s(t_i, \Theta_o) E_i^{-s} \exp \left[- \left(\frac{E_i}{E_{\text{max}}(t_i, \Theta_o)} \right)^\alpha \right] \quad (\text{A6})$$

where α is constant. The obliquity variation of K_s is given by $K_s(\Theta_o) = K_{s\parallel} \mathcal{K}(\Theta_o)$ with $\mathcal{K}(\Theta_o)$ also independent of time.

Conservation equation

$$N(E, a, t) = N(E_i, a, t_i) \frac{a^2 da dE_i}{\sigma r^2 dr dE} \quad (\text{A7})$$

(where $\sigma = n_s/n_o$) and continuity equation $n_o(a)a^2 da = n(a,t)r^2 dr$ shows that downstream

$$N(E, a, t) = K(a, t, \Theta_o) E^{-s} \mathcal{E}_{\text{rad}}(\bar{a}, E, \Theta_o)^{s-2} \times \exp \left[- \left(\frac{E \bar{a}^{3q/2}}{E_{\text{max},\parallel}(t) \mathcal{E}_{\text{ad}}(\bar{a}) \mathcal{E}_{\text{rad}}(\bar{a}, E) \mathcal{E}_{\text{max}}(\Theta_o)} \right)^\alpha \right] \quad (\text{A8})$$

with $K(a, t) = K_s(t_i) \bar{n} \mathcal{E}_{\text{ad}}^{s-1}$. If $K_s \propto V^{-b}$, then evolution of K is self-similar downstream

$$\bar{K}(\bar{a}) = K(a, t)/K_s(t) = \bar{a}^{3b/2} \bar{n}(\bar{a})^{(2+s)/3}. \quad (\text{A9})$$

Therefore, in general,

$$K(a, t, \Theta_o) = K_{s\parallel}(t) \mathcal{K}(\Theta_o) \bar{K}(\bar{a}) \quad (\text{A10})$$

where the profile $\bar{K}(\bar{a})$ is independent of obliquity. Note, that $K(a, t, \Theta_o)$ is not affected by the radiative losses, therefore it behaves in the same way also for radio emitting electrons. Once s is close to 2, the radiative losses influence the shape of $N(E)$ mostly through the exponential term in Eq. (A8). In other words, they are effective only around the high-energy end of the electron spectrum as it is shown by Reynolds (1998).

The above formulae are also valid if the spectral index s depends on E , e.g. $s(E) = s + \delta s(E)$ like it would be in case of the nonlinear acceleration. In addition, no specific value of the adiabatic index γ is assumed here. It influences the downstream evolution of relativistic electrons through $\bar{n}(\bar{a})$ which depends on γ (Sedov 1959).

APPENDIX B: APPROXIMATIONS FOR DISTRIBUTIONS OF SOME PARAMETERS BEHIND THE ADIABATIC SHOCK

Let us find approximations for dependence of some parameter $\bar{\mathcal{X}} \equiv X/X(R)$ on the Lagrangian coordinate $\bar{a} \equiv a/R$ downstream close to the adiabatic shock. We are interested in approximations of the form

$$\bar{\mathcal{X}}(\bar{a}) \approx \bar{a}^\kappa \quad (\text{B1})$$

where, by definition,

$$\kappa = \left[- \frac{a}{\mathcal{X}_*(a)} \frac{\partial \mathcal{X}_*(a)}{\partial a} \right]_{a=R} = \left[- \frac{\partial \ln \mathcal{X}_*(a)}{\partial \ln a} \right]_{a=R} \quad (\text{B2})$$

and star marks the dependence given by the Sedov solution.

This approach yields for density

$$\bar{n}(\bar{a}) \approx \bar{a}^{\kappa_{\text{na}}}, \quad \kappa_{\text{na}} = \frac{5\gamma + 13}{(\gamma + 1)^2}, \quad (\text{B3})$$

for the relation between Eulerian and Lagrangian coordinates

$$\bar{r} \approx \bar{a}^{1/\sigma}, \quad \bar{r}_{\bar{a}} \approx (1/\sigma)\bar{a}^{(1/\sigma)-1} \quad (\text{B4})$$

where the shock compression factor is

$$\sigma = \frac{\gamma + 1}{\gamma - 1}. \quad (\text{B5})$$

Note that the density distribution in Eulerian coordinates is much more sensitive to γ (Table B1):

$$\bar{n}(\bar{r}) \approx \bar{r}^{\kappa_{\text{nr}}}, \quad \kappa_{\text{nr}} = \sigma \kappa_{\text{na}} = \frac{5\gamma + 13}{(\gamma + 1)(\gamma - 1)}. \quad (\text{B6})$$

Magnetic field is approximately

$$\bar{B} \approx \bar{a}^{\beta(\Theta_{\text{o,eff}})}, \quad (\text{B7})$$

$$\beta(\Theta_{\text{o,eff}}) = \frac{\beta_{\parallel} \cos^2 \Theta_{\text{o}} + \beta_{\perp} \sigma^2 \sin^2 \Theta_{\text{o}}}{\cos^2 \Theta_{\text{o}} + \sigma^2 \sin^2 \Theta_{\text{o}}}, \quad (\text{B8})$$

$$\beta_{\parallel} = \frac{4}{\gamma + 1}, \quad \beta_{\perp} = \frac{3\gamma + 11}{(\gamma + 1)^2}. \quad (\text{B9})$$

Approximation for normalization K follows from the definition (Appendix A)

$$\bar{K} = \bar{a}^{3b/2} \bar{n}^{-(2+s)/3} \quad (\text{B10})$$

and approximation for \bar{n} .

Adiabatic losses are accounted with $\mathcal{E}_{\text{ad}}(a)$ which is defined by (A4). Its approximation is therefore

$$\mathcal{E}_{\text{ad}}(\bar{a}) \approx \bar{a}^{\kappa_{\text{ad}}}, \quad \kappa_{\text{ad}} = \frac{5\gamma + 13}{3(\gamma + 1)^2}, \quad (\text{B11})$$

it is valid for $\bar{r} > 0.8$ with error less than few per cent. The value of κ_{ad} is close to unity for $\gamma = 1.1 \div 5/3$ (Table B1).

In order to approximate \mathcal{E}_{rad} defined by (A4), we substitute (A2) with approximations for \bar{n} and \bar{B} . Then we use the property

$$\lim_{a \rightarrow 1} \left(\frac{a}{f(a)} \frac{df}{da} \right) = cy \quad (\text{B12})$$

for function of the form $f(a) = 1 - ca^x(1 - a^y)$. In this way,

$$\mathcal{E}_{\text{rad}}(\bar{a}, E) \approx \bar{a}^{\kappa_{\text{rad}}}, \quad \kappa_{\text{rad}} = \frac{5\sigma_{\text{B}}^2(\Theta_{\text{o}})E}{2E_{\text{f}\parallel}}. \quad (\text{B13})$$

This expression is good for $\bar{r} > 0.94$, with error of few per cent. It depends on γ through σ in σ_{B} which is (Reynolds 1998)

$$\sigma_{\text{B}} = \left(\frac{1 + \sigma^2 \tan^2 \Theta_{\text{o}}}{1 + \tan^2 \Theta_{\text{o}}} \right)^{1/2}. \quad (\text{B14})$$

Note that dependence on the absolute value of the magnetic field strength $B_{\text{s}\parallel}$ is present in (B13): $E_{\text{f}\parallel} \propto B_{\text{s}\parallel}^{-2}$. This approximation clearly shows that the fiducial energy E_{f} is important parameter reflecting the ‘sensitivity’ to the radiative losses, as it shown by Reynolds (1998): the larger the fiducial energy the smaller the radiative losses. In fact, $\mathcal{E}_{\text{rad}} = 1$ means no radiative losses at all, see (A4). Another fact directly visible from Eq. (B13) is that radiative losses are much more important at the perpendicular shock ($\sigma_{\text{B}} = \sigma$) than at the parallel one ($\sigma_{\text{B}} = 1$). Radiative losses depends rather strongly on the index γ : $\sigma_{\text{B}}^2 = 16$ for $\gamma = 5/3$ but $\sigma_{\text{B}}^2 = 49$ for $\gamma = 4/3$.

The values of parameters in approximations for different adiabatic index γ are presented in Table B1.

Table B1. Parameters in approximations

Expression	$\gamma = 5/3$	$\gamma = 4/3$	$\gamma = 1.1$
$\kappa_{\text{na}} = \frac{5\gamma + 13}{(\gamma + 1)^2}$	3	3.6	4.2
$\kappa_{\text{nr}} = \frac{5\gamma + 13}{(\gamma + 1)(\gamma - 1)}$	12	25	88
$\sigma = \frac{\gamma + 1}{\gamma - 1}$	4	7	21
$\beta_{\parallel} = \frac{4}{\gamma + 1}$	1.5	1.7	1.9
$\beta_{\perp} = \frac{3\gamma + 11}{(\gamma + 1)^2}$	2.2	2.8	3.2
$\kappa_{\text{ad}} = \kappa_{\text{na}}/3$	1	1.2	1.4

APPENDIX C: APPROXIMATE FORMULA FOR THE AZIMUTHAL VARIATION OF THE SYNCHROTRON X-RAY SURFACE BRIGHTNESS IN SEDOV SNR

A formula obtained here may be useful in situations when an approximate quantitative estimation for the azimuthal variation of the synchrotron X-ray surface brightness is sufficient.

1. The emissivity due to synchrotron emission is

$$q(\varepsilon) = \int N(E)p(E, \varepsilon)dE \quad (\text{C1})$$

Spectral distribution of the synchrotron radiation power of electrons with energy E in magnetic field of the strength B is

$$p(E, \nu) = \frac{\sqrt{3}e^3 B \sin \phi}{m_e c^2} F\left(\frac{\nu}{\nu_c}\right), \quad (\text{C2})$$

where ν is frequency, $\nu_c = c_1 B E^2$ the characteristic frequency. Most of this radiation is in photons with energy $\varepsilon_{\text{p}} = 0.29h\nu_c$. In the ‘delta-function approximation’, the special function F is substituted with

$$F\left(\frac{\nu}{\nu_c}\right) = \delta\left(\frac{\nu}{\nu_c} - 0.29\right) \int_0^{\infty} F(x)dx \quad (\text{C3})$$

where

$$\int_0^{\infty} F(x)dx = \frac{8\pi}{9\sqrt{3}}. \quad (\text{C4})$$

With this approximation, (C1) becomes

$$q(\varepsilon) = \frac{4\pi e^3 \sin \phi \varepsilon^{1/2} B^{1/2}}{9m_e c^2 0.29c_1^{1/2} h^{1/2}} N(E_{\text{m}}) \quad (\text{C5})$$

where E_{m} is the energy of electrons which give maximum contribution to synchrotron emission at photons with energy ε : $E_{\text{m}} = \varepsilon^{1/2} (0.29hc_1 B)^{-1/2}$.

2. Let the energy of relativistic electrons is E in a given fluid element at present time. Their energy was E_i at the time this element was shocked. These two energies are related as

$$E = E_i \mathcal{E}_{\text{ad}} \mathcal{E}_{\text{rad}} \quad (\text{C6})$$

where \mathcal{E}_{ad} accounts for the adiabatic losses and \mathcal{E}_{rad} for the radiative losses (Appendix A). There are approximations valid close to the shock (Appendix B):

$$\mathcal{E}_{\text{ad}} \approx \bar{a}^{\kappa_{\text{ad}}}, \quad \mathcal{E}_{\text{rad}} \approx \bar{a}^{5\sigma_{\text{B}}^2 E/2E_{\text{f},\parallel}} \quad (\text{C7})$$

where $\bar{a} = a/R$, a is Lagrangian coordinate of the fluid element, $E_{\text{f},\parallel}$ is the fiducial energy for parallel shock, κ_{ad} depends on γ and is given by (B11); $\kappa_{\text{ad}} = 1$ for $\gamma = 5/3$ (for other γ see Table B1). The factor σ_{B} represents compression in the classical MHD (Reynolds 1998) but may be interpreted also as amplification-plus-compression factor. In the latter case, it should be written in a way to be unity at parallel shock.

The downstream evolution of K in a Sedov SNR is (Appendix A)

$$K \propto \varsigma(\Theta_{\text{o}})\bar{K}(\bar{a}) \quad (\text{C8})$$

where ς is injection efficiency. With the approximations (C7) and s close to 2, the distribution $N(E)$ may be written from (A8) as

$$N(E, \Theta_{\text{o}}) \propto \varsigma(\Theta_{\text{o}})\bar{K}(\bar{a})E^{-s} \exp \left[- \left(\frac{E\bar{a}^{-\psi(E, \Theta_{\text{o}})}}{E_{\text{max},\parallel}\mathcal{E}_{\text{max}}(\Theta_{\text{o}})} \right)^\alpha \right] \quad (\text{C9})$$

where

$$\psi(E, \Theta_{\text{o}}) = \kappa_{\text{ad}} + \frac{5\sigma_{\text{B}}(\Theta_{\text{o}})^2 E}{2E_{\text{f},\parallel}} - \frac{3q}{2} \quad (\text{C10})$$

and s is allowed to vary with E .

3. Let us consider the azimuthal profile of the synchrotron X-ray brightness S_{ϱ} at a given radius ϱ from the center of the SNR projection.

Like in Paper II, we consider the ‘effective’ obliquity angle $\Theta_{\text{o,eff}}$ which, for a given azimuth, equals to the obliquity angle for a sector with the same azimuth in the plane of the sky (see details in Paper II). The relation between the azimuthal angle φ , the obliquity angle $\Theta_{\text{o,eff}}$ and the aspect angle ϕ_{o} is as simple as

$$\cos \Theta_{\text{o,eff}}(\varphi, \phi_{\text{o}}) = \cos \varphi \sin \phi_{\text{o}} \quad (\text{C11})$$

for the azimuth angle φ measured from the direction of ISMF in the plane of the sky.

The surface brightness of SNR projection at distance ϱ from the center and at azimuth φ is

$$S(\bar{\varrho}, \varphi) = 2 \int_{\bar{a}(\bar{\varrho})}^1 q(\bar{a}) \frac{\bar{r}\bar{r}_{\bar{a}} d\bar{a}}{\sqrt{\bar{r}^2 - \bar{\varrho}^2}} \quad (\text{C12})$$

where $\bar{r}_{\bar{a}}$ is the derivative of $\bar{r}(\bar{a})$ in respect to \bar{a} . The azimuthal variation of the synchrotron X-ray brightness is approximately

$$S_{\text{x}} \propto \varsigma(\Theta_{\text{o,eff}})\sigma_{\text{B}}(\Theta_{\text{o,eff}})^{(s+1)/2} I_{\text{rx}}(\Theta_{\text{o,eff}}, \bar{\varrho}) \times \exp \left[- \left(\frac{E_{\text{ms}}(\varepsilon, \Theta_{\text{o,eff}})}{E_{\text{max},\parallel}\mathcal{E}_{\text{max}}(\Theta_{\text{o,eff}})} \right)^\alpha \right] \quad (\text{C13})$$

where

$$I_{\text{rx}} = \int_{\bar{a}(\bar{\varrho})}^1 \frac{\bar{K}\bar{B}^{(s+1)/2}\bar{r}\bar{r}_{\bar{a}}}{\sqrt{\bar{r}^2 - \bar{\varrho}^2}} \times \exp \left[- \left(\frac{E_{\text{ms}}}{E_{\text{max},\parallel}\mathcal{E}_{\text{max}}} \right)^\alpha (\bar{a}^{-\alpha\psi(E_{\text{m}})}\bar{B}^{-\alpha/2} - 1) \right] d\bar{a}, \quad (\text{C14})$$

reflects the dependence on ρ , E_{ms} is E_{m} for $\bar{B} = 1$:

$$E_{\text{ms}}(\varepsilon, \Theta_{\text{o,eff}}) = \left(\frac{\varepsilon}{0.29hc_1 B_{\text{o}}\sigma_{\text{B}}(\Theta_{\text{o,eff}})} \right)^{1/2} \quad (\text{C15})$$

Note, that $E_{\text{ms}} \propto \varepsilon^{1/2}$, i.e. S_{ϱ} depends in our approximation on the energy ε of observed X-ray photons.

4. Let us approximate I_{rx} . First, we use the approximations $\bar{a} \approx \bar{r}^\sigma$, $\bar{K}\bar{B}^{(s+1)/2}\bar{r}_{\bar{a}} \approx \bar{a}^{\kappa_{\text{r}}}/\sigma$, which are valid close to the shock (Appendix B), σ is the shock compression ratio. Next, we expand $\bar{r}/\sqrt{\bar{r}^2 - \bar{\varrho}^2}$ in powers of the small parameter $(r - 1)$ and consider the only first term of the decomposition:

$$\frac{\bar{r}}{\sqrt{\bar{r}^2 - \bar{\varrho}^2}} \approx \frac{1}{\sqrt{1 - \bar{\varrho}^2}} \quad (\text{C16})$$

The exponential term in the integral expands in powers of the small parameter $(1 - a)$:

$$\exp(-x_1(a^{-x_2} - 1)) \approx 1 - x_1 x_2 (1 - a). \quad (\text{C17})$$

In addition, E_{ms} is used instead of E_{m} .

Close to the shock, the integral of interest is therefore

$$I_{\text{rx}}(\varphi, \bar{\varrho}) \approx I_{\text{r}}(\bar{\rho})I_{\text{x}}(\varphi, \bar{\varrho}) \quad (\text{C18})$$

where

$$I_{\text{r}} = \frac{1}{\sigma\sqrt{1 - \bar{\varrho}^2}} \frac{1 - \bar{\varrho}^{\sigma(\kappa_{\text{r}}+1)}}{\kappa_{\text{r}} + 1}, \quad (\text{C19})$$

$$I_{\text{x}} = \left[1 - \frac{\epsilon_{\text{m}}^\alpha(\psi + \beta/2)\alpha}{\mathcal{E}_{\text{max}}^\alpha} \left(1 - \frac{1 - \bar{\varrho}^{\sigma(\kappa_{\text{r}}+2)}\kappa_{\text{r}} + 1}{1 - \bar{\varrho}^{\sigma(\kappa_{\text{r}}+1)}\kappa_{\text{r}} + 2} \right) \right] \quad (\text{C20})$$

The parameter

$$\psi = \kappa_{\text{ad}} + \frac{5\sigma_{\text{B}}^2\epsilon_{\text{m}}}{2\epsilon_{\text{f},\parallel}} - \frac{3q}{2} \quad (\text{C21})$$

is responsible for the losses of emitting electrons and the time evolution of E_{max} on the shock. The value of κ_{ad} is rather close to unity for $\gamma = 1.1 \div 5/3$ (Table B1); unless radiative losses (the second term in ψ) are negligible, one may use $\kappa_{\text{ad}} \approx 1$ for any γ . Other parameters are

$$\epsilon_{\text{m}} = \frac{E_{\text{ms}}}{E_{\text{max},\parallel}} = \left(\frac{\tilde{\varepsilon}}{0.29\sigma_{\text{B}}} \right)^{1/2}, \quad (\text{C22})$$

β is given by Eq. (B8),

$$\kappa_{\text{r}} = \frac{3b}{2} + \frac{2+s}{3}\kappa_{\text{na}} + \frac{s+1}{2}\beta + \frac{1}{\sigma} - 1. \quad (\text{C23})$$

Parameters ψ , ϵ_{m} , σ_{B} , \mathcal{E}_{max} and β depend on $\Theta_{\text{o,eff}}$ and therefore on the aspect angle ϕ_{o} and the azimuth angle φ .

The parameter β reflects differences between MF distribution downstream the shock of the different obliquity. It varies from β_{\parallel} at parallel shock to β_{\perp} at perpendicular one, Eq. (B8). In the approximate formulae, it appears in the combination $\beta/2$; the role of $\beta \in [\beta_{\parallel}; \beta_{\perp}]$ is minor in modification of the approximate azimuthal and radial profiles. Therefore, in order to simplify the approximation, we may take $\beta/2 \approx 1$.

The index s in (C9), in general, is allowed to vary with E , e.g. to be $s(E) = s + \delta s(E)$. In our approximation, due to (C3), s reflects the ‘local’ slope of the electron spectrum appropriate to ϵ_{m} . Therefore, if one assumes $s(E) \neq \text{const}$, the index $s(\epsilon_{\text{m}})$ may vary with azimuth because ϵ_{m} varies, Eq. (C22).

5. The final formula is

$$S_x(\varphi, \bar{\varrho}) \propto \varsigma(\varphi) \sigma_B(\varphi)^{(s+1)/2} \exp \left[- \left(\frac{\epsilon_m(\varphi)}{\mathcal{E}_{\max}(\varphi)} \right)^\alpha \right] I_{rx}(\varphi, \bar{\varrho}; \epsilon_{f\parallel}) \quad (\text{C24})$$

where only I_x depends on $\bar{\varrho}$ and $\epsilon_{f\parallel}$.

The formula Eq. (C24) gives us the possibility to approximate both the azimuthal and the radial brightness profiles of X-ray brightness for $\bar{\varrho}$ close to unity. It may be used (with a bit larger errors compared to the case of IC emission; Fig. C1, cf. Fig. D1), for those azimuth φ where $\epsilon_m \lesssim 1$ and $\epsilon_f \gtrsim 0.1$, in the range of $\bar{\varrho}$ from $1 - 2\Delta\bar{\varrho}_m$ to 1, where $\Delta\bar{\varrho}_m = 1 - \bar{\varrho}_m$, $\bar{\varrho}_m$ is the radius where the maximum in the radial profile of brightness happens. We have in mind the maximum which is close to the shock, say $\bar{\varrho}_m > 0.95$; therefore, in order to determine $\bar{\varrho}_m$, one should look for the azimuth with the largest radiative losses. This is discussed in details on example of the IC emission in Sect. D.

Adiabatic index γ affects the approximation through σ , κ_r , κ_{ad} .

APPENDIX D: APPROXIMATE FORMULA FOR THE IC GAMMA-RAY SURFACE BRIGHTNESS IN SEDOV SNR

In Paper II, we have developed an analytic approximation for the azimuthal variation of the surface brightness of Sedov SNR in γ -rays due to the inverse-Compton process, for regions close to the forward shock. The approximation, Eq. (11), in the cited paper accounts to zeroth order. However, like in the case of the X-ray brightness, the fall of the γ -ray emissivity downstream of the shock is quite strong in case of the efficient radiative losses of electrons. Therefore, in such cases of the efficient losses we need to consider the next order of approximation.

Adopting the approach from the Appendix C to IC emission (see also some details in Paper II), we come to the approximation

$$S_{ic}(\varphi) \propto \varsigma(\Theta_{o,\text{eff}}) \exp \left[- \left(\frac{E_m(\epsilon)}{E_{\max,\parallel} \mathcal{E}_{\max}(\Theta_{o,\text{eff}})} \right)^\alpha \right] I_{ic}(\Theta_{o,\text{eff}}, \bar{\varrho}) \quad (\text{D1})$$

where the energy E_m of electrons which gives maximum contribution to IC emission at photons with energy ϵ is (e.g. Petruk 2009)

$$E_m = \frac{m_e c^2 \epsilon^{1/2}}{2(kT)^{1/2}}, \quad (\text{D2})$$

T is the temperature of the black-body photons.

The factor

$$I_{ic} = \int_{\bar{a}(\bar{\varrho})}^1 \frac{\bar{K} \bar{r} \bar{r}_a d\bar{a}}{\sqrt{\bar{r}^2 - \bar{\varrho}^2}} \exp \left[- \left(\frac{E_m}{E_{\max,\parallel} \mathcal{E}_{\max}} \right)^\alpha (\bar{a}^{-\alpha\psi} - 1) \right] \quad (\text{D3})$$

is approximately

$$I_{ic}(\varphi, \bar{\varrho}) \approx \frac{1}{\sigma \sqrt{1 - \bar{\varrho}^2}} \frac{1 - \bar{\varrho}^{\sigma(\kappa_{ic}+1)}}{\kappa_{ic} + 1} \times \left[1 - \frac{\epsilon_m^\alpha \psi \alpha}{\mathcal{E}_{\max}^\alpha} \left(1 - \frac{1 - \bar{\varrho}^{\sigma(\kappa_{ic}+2)}}{1 - \bar{\varrho}^{\sigma(\kappa_{ic}+1)}} \frac{\kappa_{ic} + 1}{\kappa_{ic} + 2} \right) \right]. \quad (\text{D4})$$

where κ_{ic} and σ comes from the approximations $\bar{a} \approx \bar{r}^\sigma$, $\bar{K} \bar{r}_a \approx \bar{a}^{\kappa_{ic}} / \sigma$,

$$\psi = \kappa_{ad} + \frac{5\sigma_B^2 \epsilon_m}{2\epsilon_{f\parallel}} - \frac{3q}{2}, \quad (\text{D5})$$

$$\epsilon_m = \frac{E_m}{E_{\max,\parallel}} = \frac{\epsilon^{1/2}}{2(kT)^{1/2} \gamma_{\max}(\varphi)}, \quad (\text{D6})$$

$$\kappa_{ic} = \frac{3b}{2} + \frac{2+s}{3} \kappa_{na} + \frac{1}{\sigma} - 1. \quad (\text{D7})$$

The final formula is

$$S_{ic}(\varphi, \bar{\varrho}) \propto \varsigma(\varphi) \exp \left[- \left(\frac{\epsilon_m}{\mathcal{E}_{\max}(\varphi)} \right)^\alpha \right] I_{ic}(\varphi, \bar{\varrho}; \epsilon_{f\parallel}) \quad (\text{D8})$$

It gives us the possibility to approximate both the azimuthal and the radial brightness profiles for $\bar{\varrho}$ close to unity.

D1 Accuracy of the approximation

Fig. D1 demonstrates accuracy of the approximation (D8) (left and middle panels show in fact the variation of I_{ic} because both ς and \mathcal{E}_{\max} are constant there). Our calculations may be summarized as follows: this approximation may be used, with errors less than $\sim 30\%$, for those azimuth φ where $\epsilon_m \lesssim 1$ and $\epsilon_f \gtrsim 0.1$, in the range of $\bar{\varrho}$ from $1 - 2\Delta\bar{\varrho}_m$ to 1, where $\Delta\bar{\varrho}_m = 1 - \bar{\varrho}_m$, $\bar{\varrho}_m$ is the radius (close to the shock) where the maximum in the radial profile of brightness happens; in addition, approximation may not be used for $\bar{\varrho} \lesssim 0.9$. If for some azimuth, the above conditions on ϵ_m and ϵ_f do not hold, the accuracy of approximation gradually decreases because the role of the exponent in $N(E)$ and of the radiative losses may not be described by the first terms in the decompositions used for derivation of the formula.

Let's consider Fig. D1. The photon energy ϵ_m does not change with azimuth for IC process. On the left panels, the reduced fiducial energy $\epsilon_f(\varphi) = \epsilon_{f\parallel} / (\mathcal{E}_{\max} \sigma_B^2) \gtrsim 0.1$ for any azimuth: $\epsilon_{f\parallel} = 3$ at the parallel shock and $\epsilon_{f\perp} = 0.19$ at the perpendicular shock. The approximation is accurate for any azimuth, for $0.98 \lesssim \bar{\varrho} \leq 1$ at $\varphi = 90^\circ$ and for a wider range of $\bar{\varrho}$ at $\varphi = 0^\circ$. Middle panels on Fig. D1 show the same case except of $\epsilon_{f\parallel} = 1$. At parallel shock (i.e. $\varphi = 90^\circ$), the range for $\bar{\varrho}$ is smaller, $0.99 \lesssim \bar{\varrho} \leq 1$ (lower panel). Therefore, the approximation of the azimuthal profile for $\bar{\varrho} = 0.98$ is inaccurate (upper panel, blue line), especially for $\varphi > 45^\circ$ where ϵ_f decreases; it is $\epsilon_{f\perp} = 0.06$. The azimuthal profile is however accurate for $\bar{\varrho} = 0.99$ (black line). Similar situation is for variable E_{\max} (right panels on Fig. D1). $E_{\max\perp} / E_{\max\parallel} = 3.25$ for considered model, therefore $\epsilon_{f\parallel} / \epsilon_{f\perp} = 52$. Therefore, in order to obtain a representative approximation, the lowest possible $\epsilon_{f\parallel}$ should be about $0.1 \times 52 = 5.2$. We see from the figure that accuracy decreases toward smaller ϵ_f (i.e. where the role of radiative losses are very efficient in modification of the electron distribution) and for smaller $\bar{\varrho}$.

In general, the accuracy of the approximation is better for larger ϵ_f and smaller ϵ_m . With decreasing of the aspect angle ϕ_o , the accuracy of the approximations for the azimuthal profile increases at the beginning (because contrasts in σ_B , ϵ_f and \mathcal{E}_{\max} are lower) and then decreases again, for the case of the quasi-parallel injection, because SNR becomes centrally-brightened while our approximation is developed for regions close to the edge of SNR.

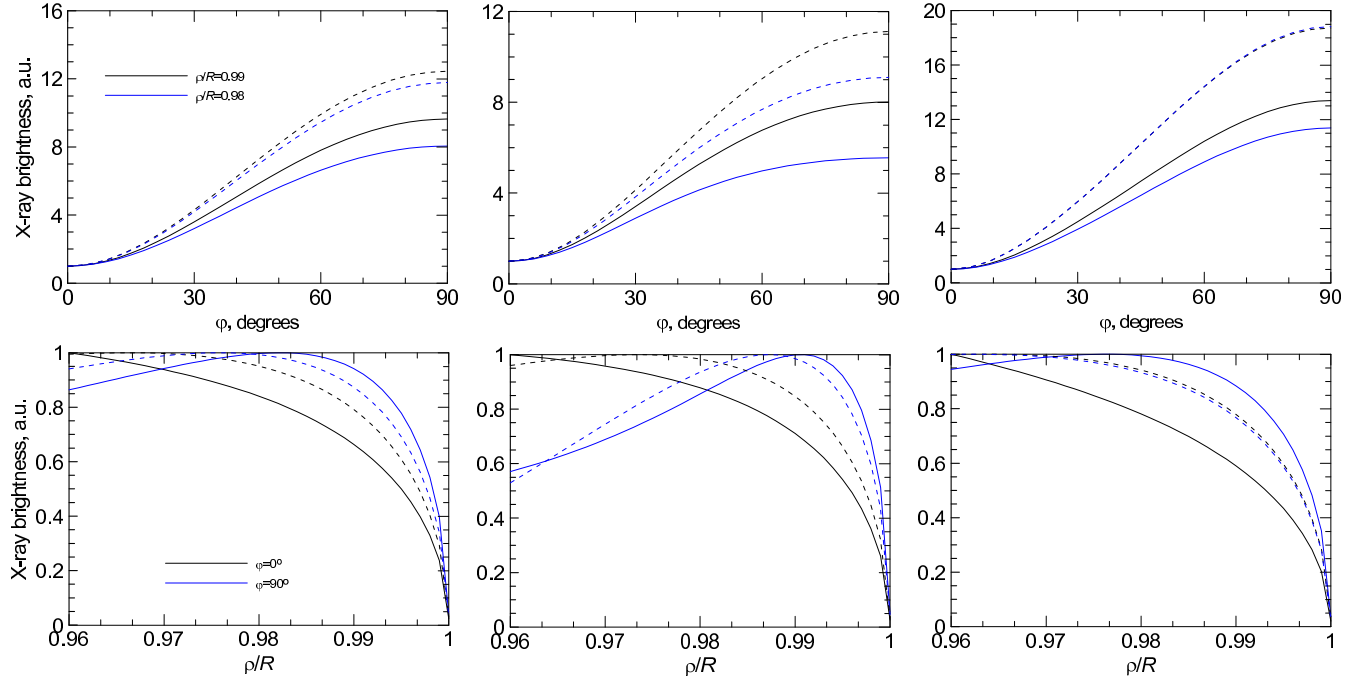


Figure C1. Azimuthal (upper panels) and radial (lower panels) profiles of the X-ray surface brightness S_x (solid lines) and its approximations (C24) (dashed lines). Calculations are done for $\phi_o = 90^\circ$, $b = 0$, isotropic injection, $\gamma = 5/3$, $s = 2$, $\alpha = 1$. Models of E_{\max} : $\mathcal{E}_{\max} = \text{const}$ (left and middle panels) and time-limited one with $\eta = 1.5$ (right panels). The reduced electron energy is $\epsilon_m = 1$ and the reduced fiducial energy is $\epsilon_{f||} = 3$ (left), $\epsilon_{f||} = 1$ (middle), $\epsilon_{f||} = 5$ (right panels).

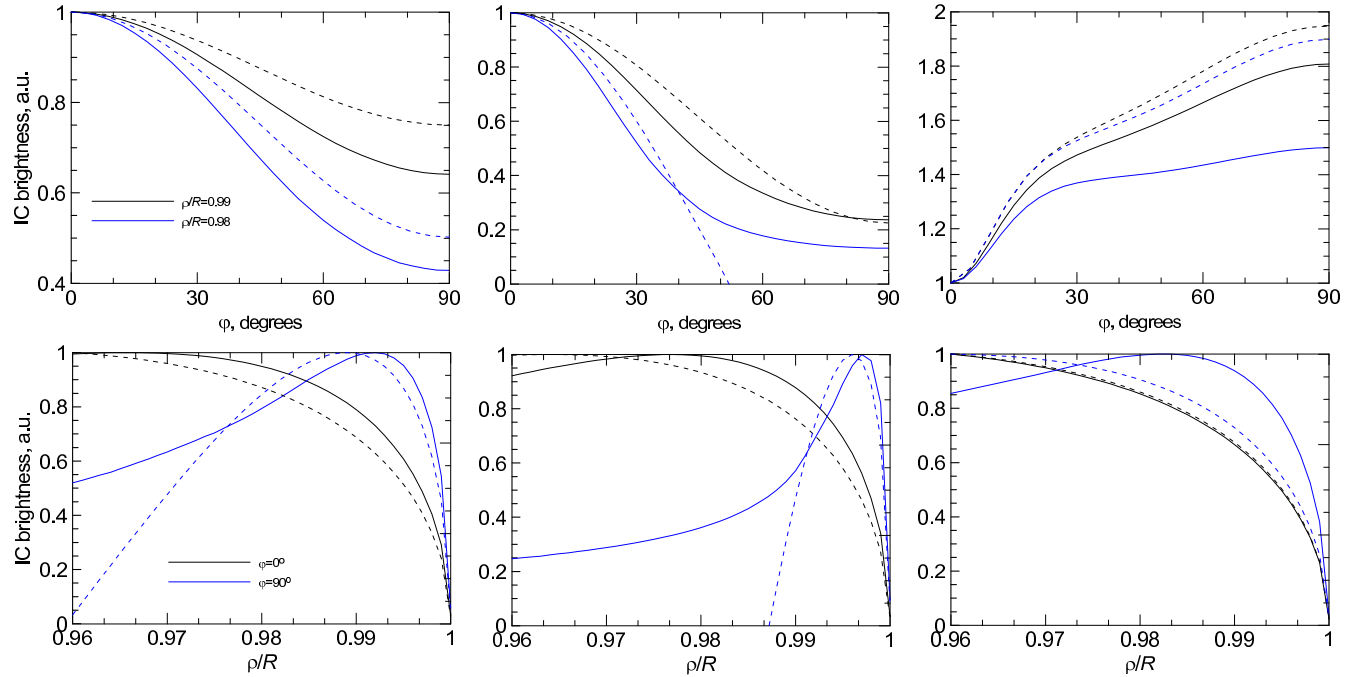


Figure D1. Azimuthal (upper panels) and radial (lower panels) profiles of the IC surface brightness S_{ic} (solid lines) and its approximations (D8) (dashed lines). Calculations are done for $\phi_o = 90^\circ$, $b = 0$, isotropic injection, $\gamma = 5/3$, $s = 2$, $\alpha = 1$. Models of E_{\max} : $\mathcal{E}_{\max} = \text{const}$ (left and middle panels) and time-limited one with $\eta = 1.5$ (right panels). The reduced electron energy is $\epsilon_m = 1$ and the reduced fiducial energy is $\epsilon_{f||} = 3$ (left), $\epsilon_{f||} = 1$ (middle), $\epsilon_{f||} = 5$ (right panels).

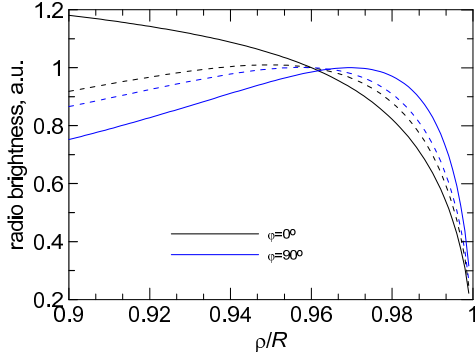


Figure D2. Radial profile of the radio brightness S_ρ (solid lines) and its approximation (C19) (dashed lines) for azimuth $\varphi = 0^\circ$ (black lines) and $\varphi = 90^\circ$ (blue lines), $\phi_o = 90^\circ$. For smaller aspects, $\phi_o < 90^\circ$, the approximation agree better with the numerical profiles.

APPENDIX E: APPROXIMATE FORMULA FOR THE RADIO SURFACE BRIGHTNESS IN SEDOV SNR

An analytic approximation for the azimuthal variation of the radio surface brightness of Sedov SNR (Paper I) may be extended to allow also for a description of the radial variation close to the forward shock. Namely, the correction consists in a factor I_r :

$$S_r(\varphi, \bar{\varrho}) \propto \varsigma(\varphi) \sigma_B(\varphi)^{(s+1)/2} I_r(\bar{\varrho}) \quad (\text{E1})$$

where I_r is the same as for the X-ray approximation (C18). Accuracy of this approximation for the radial profile of brightness is demonstrated on Fig. D2 and on Fig. 2 in Paper I for the azimuthal profiles. I_r varies with azimuth less than 10% (cf. e.g. black and blue dashed lines on Fig. D2). This variation is due only to $\beta(\Theta_o)$. Thus, β may be taken constant with a good choice $\beta/2 = 1$ (see also Appendix C).

The smaller ϕ_o , the smaller differences between the radial profiles for azimuth $\varphi = 0^\circ$ and 90° (black and blue solid lines approach one another with decrease of the aspect angle).